ELSEVIER

Chemical Engineering Journal 86 (2002) 145–151

Chemical Engineering Journal

www.elsevier.com/locate/cej

Modelling of fracture phenomena in dried materials

Stefan Jan Kowalski*

Institute of Technology and Chemical Engineering, Poznań University of Technology, pl. Marii Skłodowskiej-Curie 2, 60-965 Poznan, Poland

Abstract

Drying induced stresses may cause irreversible deformations (warping) or even fracture of dried products. This paper concerns the fracture phenomenon in capillary porous materials by drying. A short presentation of the mechanistic model of drying elaborated earlier by author is given. This model enables calculation of the drying induced stresses and their distribution in dried elements, and thus the identification of the place of maximal stress appearance. The strength of dried material, being a function of the moisture content, is determined based on the known Condon–Morse model of particle interactions. Comparison of the actual maximal stress with the admissible stress for the given material allows formulation of the fracture criterion.

Keywords: Acoustic emission; Admissible stresses; Fracture criterion; Mechanical strength

1. Introduction

The removal of moisture from capillary porous materials during drying is generally accompanied by mechanical phenomena like warping or cracking. They abate the quality of the dried products or even make them useless (see e.g. [3]). The fracture of the dried products may not occur by only very slow drying rate, but this is economically unprofitable because of long drying time. Sometimes, some plastifying agents are given to ceramic paste in order to neutralise the fracture tendency during its drying. This is, however, not possible for all dried materials.

The aim of this paper is to present a theory which enables the prediction of the drying induced stresses from one side, and the estimation of the dried material strength from the other one. Both these quantities alter during drying. Three items are discussed: first, the distribution of drying induced stresses and their evolution in time; second, the strength of the dried material and the criterion of fracture; and third, the acoustic emission as a method for experimental analysis of the fracture phenomenon.

The theory presented in this paper refers rather to materials that before drying have a condensed dispergate consistence, as for example, solid suspensions, ceramic pastes used for production of electronic elements, clay for bricks production, etc. These media after drying and calcination become porous with relatively high mechanical strength.

The admissible stress of dried body is determined, based on the model of particle interactions expressed by the Condone–Morse curves. If the stress concentrated at the flaw (pore) tip is greater than the admissible one, the fracture of the body can take place. Thus, the fracture criterion is derived from the comparison of the maximal stress in the body and the determined admissible stress. Besides, basing on the Griffith concept, a critical length of the flaw that may grow spontaneously at a given stress is estimated.

Finally, the acoustic emission is indicated as a possible experimental method for identification of the fracture intensity during drying. It enables observation of the amplitude distribution of acoustic signals showed the scale of the failure phenomenon.

2. Mechanistic model of drying

One assumes that materials under drying are generally composed of three immiscible phases: porous solid (S), liquid (L), and gas (G). The gas phase is a miscible mixture of vapour (V) and air (A) (see [16]). The construction of mechanistic theory of drying is based on balance equations of mass, momentum, energy, and entropy, and the principles of thermodynamics of irreversible processes. For details, the reader is asked to refer to the author's previous papers as, e.g. [4–8,12]. Here, only a final form of these equations is presented.

The first fundamental set of equations comes from the mass balance, and is of the form

$$\dot{\rho}^{\alpha} = -\rho^{\alpha}\dot{\varepsilon} - W^{\alpha}_{i,i} + \hat{\rho}^{\alpha}, \qquad \alpha = \mathrm{S, L, V, A} \tag{1}$$

These equations state that the time alteration of αth constituent mass inside the dried body per unit total volume is

* Tel.: +48-61-665-3622; fax: +48-61-665-3649.
E-mail address: kowal@rose.man.poznan.pl (S.J. Kowalski).

1385-8947/02/$ – see front matter
PII: S1385-8947(01)00282-0

caused by the volume change (first term on r.h.s.), efflux or influx of this mass through the boundary surface (second term on r.h.s.), and the phase transitions (third term on r.h.s.). It is obvious that $\hat{\rho}^{\mathrm{S}} = 0$, $\hat{\rho}^{\mathrm{A}} = 0$, $\hat{\rho}^{\mathrm{L}} + \hat{\rho}^{\mathrm{V}} = 0$, $W_i^{\mathrm{S}} = 0$. Here, $\varepsilon = u_{i,i}$ denotes the volumetric strain and u_i the displacement of the solid body. The mass balance equations allow us to calculate the moisture content alteration during drying if the rate equations for constituent flux W_i^{α} and the phase transition $\hat{\rho}^{\alpha}$ are known.

The constituent flux was stated to be proportional to the gradient of constituent potential μ^{α}, diminished by the gravity force (acceleration) g_i, i.e.

$$W_i^{\alpha} = -\Lambda^{\alpha}(\mu^{\alpha}_{,i} - g_i) \quad \text{with} \quad \Lambda^{\alpha} \geq 0 \tag{2}$$

The rate of phase transition of liquid into vapour was stated to be proportional to the difference between the constituent potentials, i.e.

$$\hat{\rho}^{\mathrm{L}} = -\hat{\rho}^{\mathrm{V}} = -\omega(\mu^{\mathrm{L}} - \mu^{\mathrm{V}}) \quad \text{with} \quad \omega \geq 0 \tag{3}$$

The constituent potential is, in general, a function of parameters of state: temperature T, volumetric strain ϵ, and the specific constituent content $X^{\alpha} = \rho^{\alpha}/\rho^{\mathrm{S}}$, i.e.

$$\mu^{\alpha} = \mu^{\alpha}(T, \varepsilon, X^{\alpha}) \tag{4}$$

The balance of momentum is reduced here as the acceleration and the kinetic energy of the dried body are assumed to be negligibly small. Thus, the equation of momentum balance expresses the internal equilibrium of surface forces (stresses) and the gravitational forces, i.e.

$$\sigma_{ji,i} + \rho g_i \approx 0, \quad \rho = \sum_{\alpha} \rho^{\alpha} \tag{5}$$

where σ_{ji} is the total stress tensor. Eq. (5) serves us, after substituting the physical relations, for description of the dried body deformation and the drying induced stresses. The physical relation, in the case of reversible deformation by drying or wetting, has the form (see [8])

$$\sigma_{ij} = 2M\varepsilon_{ij} + \left\lfloor A\varepsilon - \gamma^{\mathrm{T}}(T - T_0) - \gamma^{\mathrm{X}} X^{\mathrm{L}} \right\rfloor \delta_{ij} \tag{6}$$

where $\varepsilon_{ij} = \frac{1}{2}(u_{i,j} + u_{i,j})$ is the strain tensor, M and A the shear and bulk moduli of the dried body, $\gamma^{\mathrm{T}} = (2M + 3A)\alpha^{\mathrm{T}}$, $\gamma^{\mathrm{X}} = (2M + 3A)\alpha^{\mathrm{X}}$, and α^{T} and α^{X} denote the coefficients of thermal and swelling (shrinking) expansion, respectively. It was assumed in Eq. (6) that only the moisture in liquid phase influences the shrinkage by drying, and thus the stresses.

The equation of energy balance, after suitable reductions, enables calculation of the temperature field in the dried body. Its form is as follows:

$$\rho^{\mathrm{S}} \dot{s} T = (\Lambda^{\mathrm{T}} T_{,i})_{,i} + R + \Omega \tag{7}$$

where Λ^{T} is the coefficient of heat conduction, R the volumetric heat supply (radiation), Ω the heat source. Entropy s of the whole body, referred to the mass of the dry body, is a function of the parameters of state

$$\dot{s} = \dot{s}(T, \varepsilon, X^{\mathrm{L}}) = \frac{c_{\mathrm{v}}}{T}\dot{T} - \gamma^{\mathrm{T}}\dot{\varepsilon} + C^{\mathrm{X}}\dot{X}^{\mathrm{L}} \tag{8}$$

The heat sources arise from the phase transition and the irreversible moisture movement

$$\Omega = \omega(\mu^{\mathrm{L}} - \mu^{\mathrm{V}})^2 + \sum_{\alpha} \Lambda^{\alpha} |\mu^{\alpha}_{,i} - g_i|^2 \tag{9}$$

The above system of equations is a complete one to calculate the reversible deformations of the dried body, and the drying induced stresses caused by the moisture removal and the temperature field. This system has to be supplemented by the initial and the boundary conditions.

The initial conditions state the initial value of the temperature, the moisture content, and the deformation or the state of stress. The boundary conditions state the boundary value for stresses or deformations and the conditions for heat and mass transfer. The mechanical boundary condition assumes the stress free boundary surface (absence of external forces). The mass transfer boundary condition determines the convective mass exchange, i.e.

$$W_n^{\mathrm{L}} = -\Lambda^{\mathrm{L}} \mu^{\mathrm{L}}_{,i}|_{\partial B} = \kappa^{\mathrm{V}}(\mu_n^{\mathrm{V}} - \mu_{\infty}^{\mathrm{V}}) \tag{10}$$

where κ^{V} is the coefficient of the convective vapour transfer, μ_n^{V} and $\mu_{\infty}^{\mathrm{V}}$ the vapour potentials in the drying medium (air) at the boundary and far from it, respectively.

The boundary condition for convective heat transfer, e.g., is

$$-\Lambda^{\mathrm{T}} T_{,i}|_{\partial B} = \kappa^{\mathrm{T}}(T_{\infty} - T|_{\partial B}) - l W_n^{\mathrm{V}} \tag{11}$$

where κ^{T} is the coefficient of the convective heat transfer, l the latent heat of evaporation, T_{∞} the temperature of the drying medium (air) far from the boundary.

3. Numerical example

A simple numerical example is presented to illustrate the application of the above model for the calculation of the drying induced stresses in a convectively dried bar having rectangular cross-section. It is known that maximal stresses by drying of ceramic-like materials arise during the first period of drying. Therefore, the considerations are referred to the first period of drying, in which the material is fully saturated, and the main phase transition of water into vapour proceeds on the boundary. Details concerning the adoption of the general model to this particular boundary value problem can be find, e.g., in [9–11], and the numerical method in [13].

Fig. 1 illustrates the isolines of normal stresses in a quarter cross-section of the bar (symmetrical problem), at instances of $t_1 = 40$ min and $t_2 = 90$ min. The isolines allow us to identify the place where the maximal stresses are induced. It can be seen that the biggest tensile stresses are on the boundary surfaces in the middle of cross-section

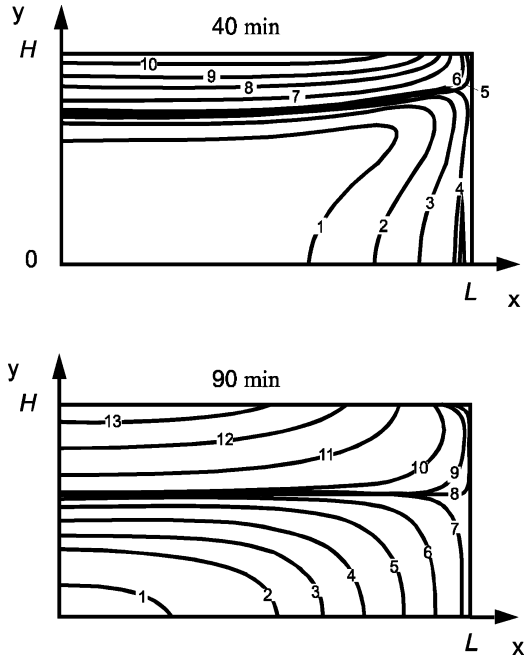

Fig. 1. Isolines of normal stresses σ_{xx} at instances 40 and 90 min of a drying process.

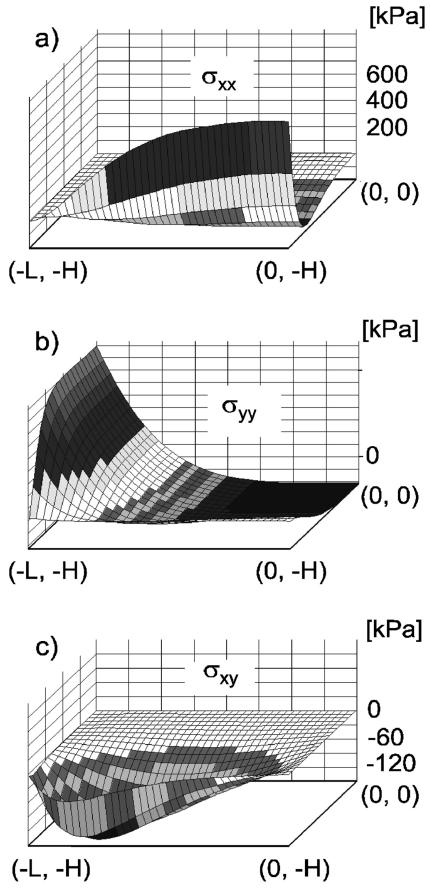

Fig. 2. Distribution of stress: (a) σ_{xx}, (b) σ_{yy}, and (c) σ_{xy} after 5 h of drying.

($\sigma_{xx} = 385$ kPa for isoline 10 in the upper figure). As the internal forces have to be semi-balanced, it is obvious that both tensile and compressive stresses arise in the cross-section. The isoline of zero-value stress separates the positive (tension) and negative (compression) stresses. The area of tension stresses at the beginning is smaller than the area of compressive stresses, however, the values of tensile stresses are significantly bigger than the compressive ones. In the course of drying the isoline of zero-value stress displaces towards the interior of the cross-section. The stresses decrease when the distribution of the moisture content in the cross-section becomes more uniform.

Fig. 2 shows a spatial visualisation of normal stresses σ_{xx}, σ_{yy} and shear stresses σ_{xy} in the cross-section after 5 h of drying. Again, it is seen that the normal stresses are tensional near the boundaries and compressional inside the cross-section. The tensional stresses are maximal in the middle of boundary surfaces and the biggest are those on the longer side of the cross-section. The shear stresses appear near the corners and are maximal when the difference between normal stresses achieves maximal value.

4. Strength of dried materials

A number of materials before drying have a condensed dispergate structure, as for example, ceramic pastes, clay, etc. Such materials after drying and calcination become porous with relatively high mechanical strength.

The dispergate systems are characterised by large interfacial surfaces, and thus also surface energy, which is the main reason for aggregation of particles. The liquid bridges between adjoining particles due to capillary pressure make additional attractive forces, which enhances aggregation. The values of capillary forces are comparable with those of London's ones at atomic contacts.

Let us imagine two adjoining elementary particles placed on the opposite sides of the cross-section α–α of a tensed bar (Fig. 3a). If the tension force between particles A_1 and A_2 is F, then the stress $\sigma = F/A$ is approximately F/L_0^2, and the strain equals $\varepsilon = (L - L_0)/L_0$. For stretching of the two adjoining particles by dL, the stress increment is

$$\mathrm{d}\sigma = \frac{1}{L_0^2}\left(\frac{\partial F}{\partial L}\right)_{L=L_0} \qquad \mathrm{d}L = E\,\mathrm{d}\varepsilon \tag{12}$$

where $E = L_0^{-1}(\partial F/\partial L)_{L=L_0}$ denotes the modulus of elasticity.

Fig. 3b illustrates the curves of displacements of two particles. Let the equilibrium position of two particles in dry state is 1 and 2, and in the saturated (swelled) state 1 and 2″. In a saturated state the distance between particles is L''. Due to drying and shrinking the particles displace closer to each other, e.g., from position 2″ to 2 for the free shrinkage, or from position 2″ to 2′ for the constrained (not free)

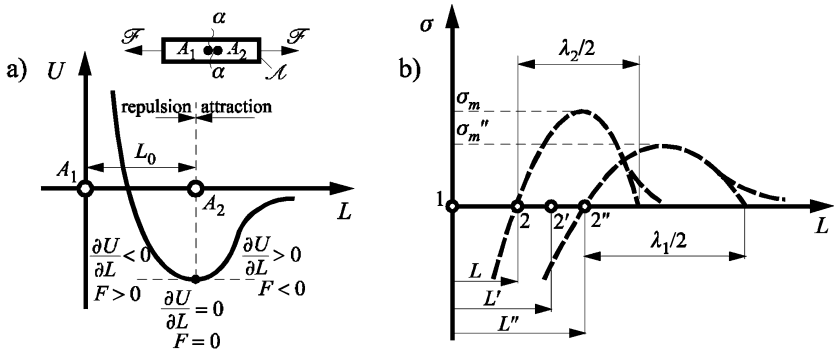

Fig. 3. Condon–Morse curves: (a) variation of potential energy versus interatomic distance; (b) stress σ by tension of samples of different saturation.

shrinkage. The constrained shrinkage takes place in the presence of stresses that counteract the shrinkage phenomenon.

Let X denotes the current moisture content of the dried body, and $L(X)$ and $L'(X)$ the distances between two particles at the stress-free state and non-zero state of stress, respectively. Mechanical strain involved by this stress reads

$$\varepsilon^{\mathrm{M}} = \frac{L'(X) - L(X)}{L(X)} = \frac{1}{E(X)}\sigma \tag{13}$$

where Young's modulus $E(X)$ is a function of the current moisture content.

Fig. 4a performs a possible stress–strain relation for a saturated porous material. The compliance of this material (inverse of Young's modulus) is assumed to be a linear function of the moisture content. Thus, the Young's modulus depends on the moisture content in the following way:

$$E(X) = \frac{E_0}{1 + aE_0(X - X_0)} \tag{14}$$

where E_0 is the Young's modulus for dry body of final moisture content X_0, and a the coefficient of influence of the moisture content on the compliance. Fig. 4b illustrates this relation for various values of coefficient a.

The boundary of the body tends to shrink during drying but is restrained by the wet core. The boundary surface is tensed and the core compressed. The tension stresses may involve fracture on the surfaces. The tension curves for materials of different moisture content are shown in Fig. 3b. The curve has a shape which is possible to approximate with the sine function (see, e.g. [1,14]).

$$\sigma = \sigma_{\mathrm{m}} \sin\left(\frac{2\pi u}{\lambda}\right) \tag{15}$$

where σ_{m} denotes the admissible maximal stress for the material, $u = L' - L$ the displacement equivalent to the applied stress, and λ the period of the sine function being dependent on the moisture content.

The magnitude of σ_{m} can be quantified in terms of work necessary to apply to the material to displace particles for a distance of $\frac{1}{2}\lambda$, at which their permanent separation takes place. This work is expressed by the following integral:

$$U = \int_0^{\lambda/2} \sigma \, \mathrm{d}u = \int_0^{\lambda/2} \sigma_{\mathrm{m}} \sin\left(\frac{2\pi u}{\lambda}\right) \mathrm{d}u = \frac{\lambda\sigma_{\mathrm{m}}}{\pi} = \frac{2L(X)}{E(X)}[\sigma_{\mathrm{m}}(X)]^2 \tag{16}$$

where λ in the above formula was replaced by the expression derived from the condition

$$\left.\frac{\mathrm{d}\sigma}{\mathrm{d}u}\right|_{u=0} = \sigma_{\mathrm{m}}\frac{2\pi}{\lambda} = \frac{E}{L} \tag{17}$$

Assuming that the energy lost for plastic deformations and reconstruction of crystal lattice during the material fracture is

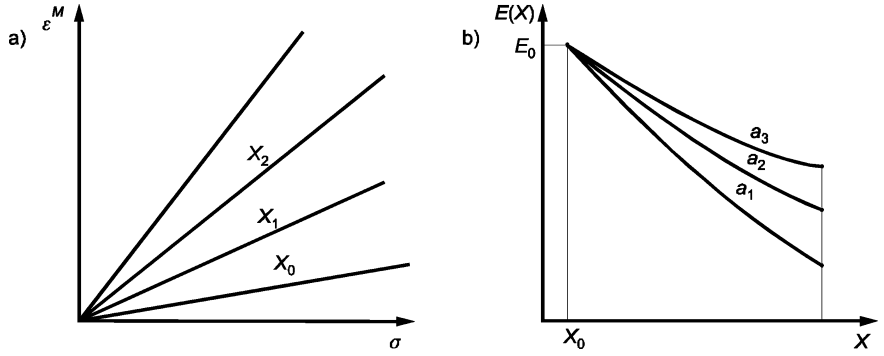

Fig. 4. Influence of sample saturation on: (a) relation between strain and stress; (b) Young's modulus.

negligible, then the energy of the two newly created surfaces 2γ is, according to Griffith's theory, equal to the applied work U.

The above statement allows writing the yield stress as a function of moisture content, viz.

$$\sigma_{\mathrm{m}}(X) = \sqrt{\frac{\gamma E(X)}{L(X)}} \tag{18}$$

where $L(X) = L_0[1 + \alpha_{\mathrm{X}}(X - X_0)]$ is the inter-particle distance in a wet material of moisture content X, and α_{X} the coefficient of linear shrinkage.

The increase of the theoretical strength during drying processes results from two reasons: increasing of Young's modulus, and diminishing of distances between particles.

5. Fracture

Fracture in porous media appears mostly at the tips of flaws or pores where the stress is concentrated, see Fig. 5. The stress σ_{c} concentrated at the flaw tip of length c and radius r (see e.g. [14,15]) can be written as

$$\sigma_{\mathrm{c}} = \sigma(1 + 2\sqrt{c/r}) \tag{19}$$

where σ is the average macroscopic stress acting on the network.

One assumes that the fracture may occur when the stress σ_{c} is greater that the yield strength σ_{m}, what allows us to write

$$\sigma > \sqrt{\frac{\gamma E(X)}{L(X)}} \frac{1}{1 + 2\sqrt{c/r}} \approx \sqrt{\frac{\gamma E(X) r}{2cL(X)}} \tag{20}$$

The above fracture criterion is suitable for strongly tensed boundary surfaces.

Let us consider a sample in the form of thin plate having a thin flaw (crack) in the middle, Fig. 5b. Let the sample be tensed with the macroscopic stress σ in the direction perpendicular to the flaw axis. The mechanical work supply to the sample due to action of this stress equals the total energy per unit thickness accumulated in the sample [2]

$$U = U_0 - \frac{\pi\sigma^2 c^2}{E} + 2\gamma(2c) \tag{21}$$

where U_0 is the energy of this sample without flaw. The second term expresses a reduction of the sample energy because of flaw, and the third one expresses the additional energy due to two flaw surfaces.

The flaw may increase its size spontaneously, but only when a decrease of energy during this process takes place, i.e. $(\partial U/\partial c) \leq 0$. It is obvious because the negative term in (21) contains the flaw dimension to second power, while the flaw dimension in the third (positive) term is only to first power.

Differentiating (21) with respect to c one can find the critical length of the flaw c_{cr}

$$c_{\mathrm{cr}} = \frac{2\gamma E}{\pi\sigma^2} \tag{22}$$

The fracture process will proceed spontaneously at the given stress σ for all flaws of dimension $c > c_{\mathrm{cr}}$. Practically, one foresees that the fracture will proceed at the yield stress σ_{m} when dimension of the flaw equals about six interatomic distances.

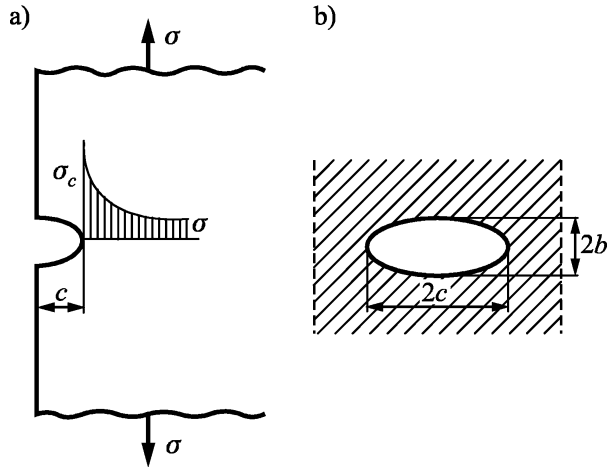

Fig. 5. Concentration of stresses.

6. Experimental identification of fracture

Material fracture generates some kind of elastic waves. Such waves appear also in saturated materials during their drying, if the drying induced stresses exceed admissible values. This is manifested by the emission of acoustic signals (EA) detected by the special receivers. Some signals can be even audible for human being in a form of clicks if the energy released by cracking is enough large, or not audible if this energy is small. Before the macroscopic cracks releasing high energy arise in the material, they are preceded by the not audible ultrasonic waves generated by micro-cracks. The registration of ultrasonic waves is possible by very sensitive receivers after strengthening of the acoustic signals. The method of registration of sonic signals generated by the fracture and micro-cracking of the structure is termed the acoustic emission method (EA).

Figs. 6–9 illustrate some results obtained from the acoustic emission (EA) measurements during drying process of a cylindrical sample made of ceramic-like material. Fig. 6 presents the number N_i of acoustic signals per 30 s, emitted during 220 min drying process. It is visible that during the first 80 min the number of EA signals is great. Probably, most of the signals are due to reformulation of the material grains and micro-cracks. We can state so because the energy of these EA signals in this range of drying is rather small, as it is seen in Fig. 7. In the course of time, the number N_i decreases (Fig. 6) but their energy (Fig. 7) increases. This is

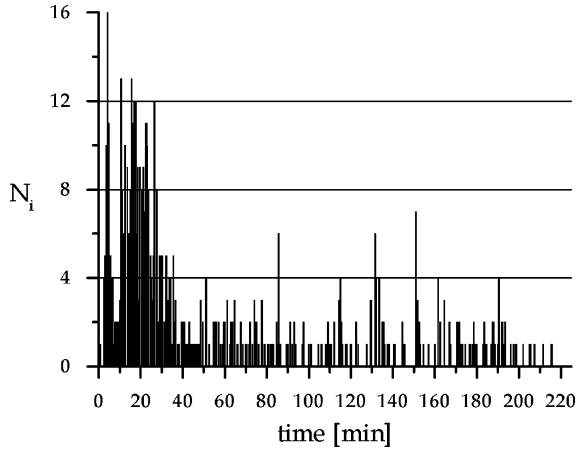

Fig. 6. Number of EA signals per 30 s versus time.

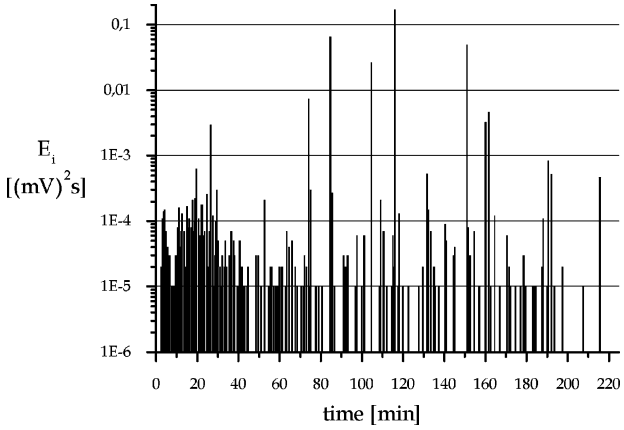

Fig. 7. Energy of EA signals per 30 s versus time.

clearly visible in Figs. 8 and 9. The former presents the total number of EA signals, counted from the beginning of the drying process, and latter the total amount of energy emitted by dried material during that time. We see a rapid increase

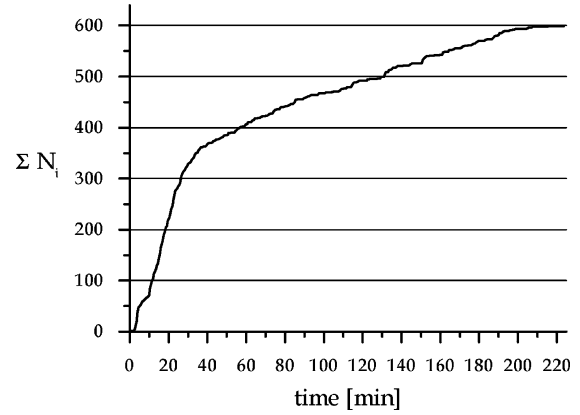

Fig. 8. Total number of EA impulses counted from the beginning of drying process.

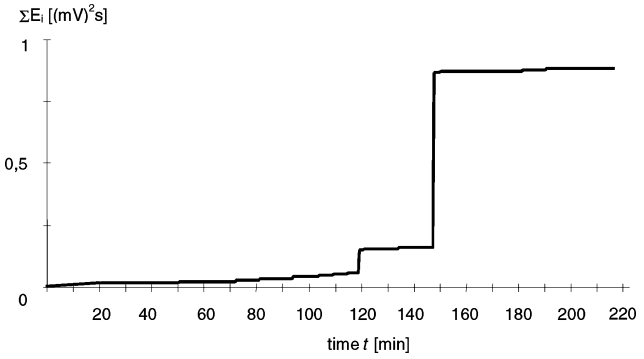

Fig. 9. Total amount of energy emitted by dried material from the beginning of drying process.

of EA signals in the first stage of drying and a moderate increase in the further stage of drying. As far as it concerns the energy, its significant increase is visible in a later stage of drying. During the test registered in Fig. 9 the rapid increase of energy took place in 150 min of drying time. The surface macro-cracks, visible with naked eye, appeared in this case. During optimal program of drying (not described here) the receiver of EA did not register of higher amplitude signals generated by the macro-cracks.

7. Final remarks

The problem of fracture during drying processes was discussed in this paper. To describe this phenomenon the mechanistic model of drying, that enables calculation of the drying induced stresses, was given, and the admissible stress for dried material at a given stage of drying process was determined by making use the Condon–Morse interaction curves. The fracture may proceed if the maximal stress in the body overcome the admissible stress. Finally, the acoustic emission was suggested as the method suitable for experimental identification of fracture intensity.

Concluding, one can state that fracture is more likely if the dried body is thick and/or the drying rate is high. These circumstances involve great inhomogeneity in moisture distribution and induce great stresses. The cohesion force, on the other hand, is proportional to the body particle size and inversely proportional to the square of the inter-particle distance. It means that the cohesion force between body particles decreases evidently with increase of the moisture content, which causes the porous body to swell. The cohesion forces determine the admissible stress.

Acknowledgements

This work was carried out as a part of research project DS 32/013/2000 at Poznań University of Technology.

References

[1] A.H. Cottrell, The Mechanical Properties of Matter, PWN, Warszawa, 1970 (in Polish).
[2] A.A. Griffith, The Phenomena of Rupture and Flow in Solids, Engineering Royal Aircraft Establishment, 1920, pp. 163–198.
[3] M. Hasatani, Y. Itaya, in: A.S. Mujumdar (Ed.), Effect of Drying Process on Quality Control in Ceramic Production, Drying'92, 1992.
[4] S.J. Kowalski, Thermomechanics of constant drying rate period, Arch. Appl. Mech. 39 (3) (1987) 157–176.
[5] S.J. Kowalski, Thermomechanics of dried materials, Arch. Appl. Mech. 42 (2) (1990) 123–149.
[6] S.J. Kowalski, Thermomechanics of drying process of fluid-saturated porous media, Drying Technol. 12 (4) (1994) 453–482.
[7] S.J. Kowalski, Drying processes involving permanent deformations of dried materials, Int. J. Eng. Sci. 34 (13) (1996) 1491–1506.
[8] S.J. Kowalski, Toward a thermodynamics and mechanics of drying processes, Chem. Eng. Sci. 55 (2000) 1289–1304.
[9] S.J. Kowalski, G. Musielak, Deformations and stresses in dried wood, Transport in Porous Media 34 (1999) 239–248.
[10] S.J. Kowalski, A. Rybicki, Drying stress formation by inhomogeneous moisture and temperature distribution, Transport in Porous Media 24 (1996) 139–156.
[11] S.J. Kowalski, A. Rybicki, Computer simulation of drying. Optimal control, Transport in Porous Media 34 (1999) 227–238.
[12] S.J. Kowalski, Cz. Strumillo, Moisture transport, thermodynamics, and boundary conditions in porous materials in presence of mechanical stresses, Chem. Eng. Sci. 52 (7) (1997) 1141–1150.
[13] R.W. Lewis, M. Strada, G. Comini, Drying-induced stresses in porous bodies, Int. J. Numer. Meth. Eng. 11 (1977) 175–1184.
[14] R. Pampuch, Ceramic Materials, PWN, Warszawa, 1988 (in Polish).
[15] L.I. Siedov, Mechanics of Continua, Nauka, Moscow, 1984 (in Russian).
[16] Cz. Strumillo, T. Kudra, Drying: Principles, Applications and Design, Gordon and Breach, New York, 1986.